Wireless Power Transfer: A Paradigm Shift for the Next Generation

Shu-Yuen Ron Hui, *Fellow, IEEE*, Yun Yang, *Member, IEEE*, and Cheng Zhang, *Member, IEEE*

(Invited Paper)

***Abstract*— The first generation of wireless power transfer (WPT) standard Qi, launched in 2010, contains a wide range of transmitter and receiver designs with the aim of maximizing compatibility to attract many manufacturers to share the same standard. Such compatibility feature (i.e., interoperability) has not only attracted over 400 company members in the Wireless Power Consortium (WPC), but also facilitated a fast-growing wireless power market for a decade. The WPC is now expanding the scope of WPT applications to mid-power and high-power applications up to several kilowatts while the Society for Automobile Engineers (SAE) also set the SAE standard for wireless charging of electric vehicles (EVs) up to tens of kilowatts. Without compromising compatibility, the authors share in this article their views on the need for a paradigm shift from compatibility to optimal performance in terms of maximum energy efficiency for the entire charging process and minimum charging time. This paradigm change is imminent and important in view of the increasing power of WPT applications. Several enabling technologies essential to the paradigm shift will be addressed.**

***Index Terms*— New paradigm shift, wireless power transfer (WPT).**

I. Introduction

With the launch of the world's first wireless standard Qi in 2010 by the Wireless Power Consortium (WPC), wireless charging technologies have been widely adopted in portable consumer electronics, such as mobile phones. Up to 2020, mobile phones of all major brands are Qi-compatible, and many car manufacturers offer wireless charging pads as standard or optional equipment in new vehicles. The wireless power market has reached US $12.7 billion by 2020 and is expected to exceed 185 billion by 2030, according to Statista [1]. As the popularity of wireless power transfer (WPT) applications continues to grow, the WPC [2] is planning to extend the scope of WPT applications to cover mid-power and high-power applications, such as portable electric tools, light electric vehicles (LEVs), kitchen appliances and industrial robotics and auto-guided vehicles (AGVs) and unmanned underwater vehicles (UUVs). The Society of Automobile Engineers (SAE) has published the SAE J2954 for wireless charging of electric vehicles (EVs) up to 11 kW [3]. While the operating frequencies of the standards developed by the WPC and SAE are less than 1 MHz, another organization, the AirFuel Alliance, suggests the use of 6.78 MHz for WPT applications [4]. Fig. 1 shows the existing power-frequency regions of WPT applications currently covered by WPC, SAE, and AirFuel. It is noted that there is still largely uncharted territory in the high-power and high-frequency regions.

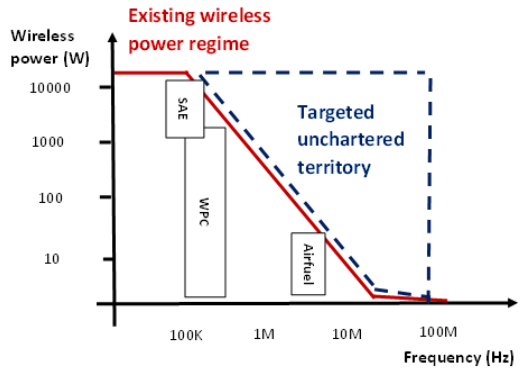

Fig. 1. Power-frequency regions used by SAE, WPC, and AirFuel alliance for near-field magnetic-resonance-based WPT applications.

For the first generation of WPT standards, such as Qi and SAE J2954, "compatibility" among various transmitter and receiver designs is critical in attracting companies and manufacturers to take part in using the standards. The information in Table I illustrates the strong focus on the compatibility of Qi based on Version 1.2.3 of Qi published in February 2017, which comprises 50 transmitter designs and five receiver designs. In this regard, the Qi standard has been very successful in the commercialization of WPT products because the company members of the WPC have exceeded 430 and over 14 000 electronics products have been

Manuscript received 6 July 2022; revised 30 November 2022 and 6 January 2023; accepted 7 January 2023. Date of publication 23 January 2023; date of current version 13 June 2023. This work was supported in part by the Singapore Agency for Science, Technology and Research (A*Star) Manufacturing, Trade and Connectivity-Individual Research Grant (MTC-IRG) under Grant M21K2c0108. Recommended for publication by Associate Editor Don F. D. Tan. *(Shu-Yuen Ron Hui, Yun Yang, and Cheng Zhang are co-first authors.) (Corresponding author: Shu-Yuen Ron Hui.)*

Shu-Yuen Ron Hui is with the School of Electrical and Electronic Engineering, Nanyang Technological University, Singapore 639798, and also with the Department of Electrical and Electronic Engineering, Imperial College London, South Kensington, SW7 2AZ London, U.K. (e-mail: ron.hui@ntu.edu.sg).

Yun Yang is with the School of Electrical and Electronic Engineering, Nanyang Technological University, Singapore 639798 (e-mail: yun.yang@ntu.edu.sg).

Cheng Zhang is with the Department of Electrical and Electronic Engineering, University of Manchester, M13 9PL Manchester, U.K. (e-mail: cheng.zhang@manchester.ac.uk).

Color versions of one or more figures in this article are available at https://doi.org/10.1109/JESTPE.2023.3237792.

Digital Object Identifier 10.1109/JESTPE.2023.3237792

This work is licensed under a Creative Commons Attribution-NonCommercial-NoDerivatives 4.0 License.
For more information, see https://creativecommons.org/licenses/by-nc-nd/4.0/

TABLE I
NUMBERS OF TRANSMITTER AND RECEIVER DESIGNS IN QI STANDARD V.1.2.3 (2017)

	Number	Total
Transmitter designs with single coil excitation (Tx: A1 – A34)	34	50
Transmitter design with multiple-coils excitation (Tx: B1-B7)	7	
Transmitter design with extended power profile (Tx: MP-A1 – MP-A8, MP-B1)	9	
Receiver designs	5	5

registered as Qi-compatible, and over 9000 Qi-compatible products commercially available in the market by 2022.

As the power level of emerging WPT applications continues to increase, the authors believe that there is a need to shift the paradigm *from "compatibility" to "optimal performance" in terms of 1) maximum energy efficiency and 2) minimum charging time for the entire battery charging process while retaining compatibility as a basic element*. In this article, the authors share their views on the next generation of WPT research and developments. These include how the paradigm shift can be achieved with emerging technologies and how to break into the unchartered territory of high-power (kW) and high-frequency (MHz) WPT operating regions. The proposed paradigm shift from compatibility to both optimal performance and compatibility is applicable to a wide range of near-field magnetic-resonance-based WPT applications, regardless of the WPT standards, power levels, and operating frequencies suggested by different WPT organizations.

With the understanding that it is impossible to cover all aspects of emerging WPT technologies, this article focuses on the following aspects that the authors believe to be highly relevant to achieving the new paradigm shift (Fig. 2) for the next generation.

1) To establish a common principle of transferring most of the control functions to the transmitter (primary) side so that the manufacturers of the transmitters would be responsible for optimal performance in terms of maximizing the energy efficiency and minimizing the charging time, while the receiver circuits retain basic functions, such as protection against over-voltage, over-current and over-temperature conditions in the battery loads. This paradigm shift is illustrated in Fig. 2.
2) To develop a fast and accurate primary-side monitoring method to determine mutual coupling coefficient, unknown parameters of the receiver circuits, and battery conditions based on primary-side measurements.
3) To develop an accurate battery twin incorporating electrical, thermal, and chemical characteristics and then to apply maximum efficiency point tracking (MEPT) in the primary-side control for optimal performance of maximum efficiency and minimum charging time for the entire battery charging process.
4) For the breakthroughs in the high-frequency (MHz) and high-power regime, to develop new gate drives with soft-switching capability and minimum latency for emerging wide bandgap (WBG) power devices and to design new high-frequency resonator structures with minimum intercapacitance and intracapacitance and ac resistance.

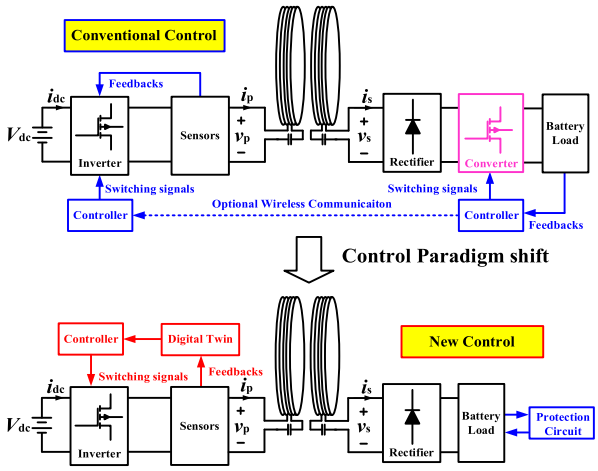

Fig. 2. Schematic of a control paradigm shift for the next-generation WPT.

Section II of this article describes several MEPT methods to achieve the first optimal performance of maximum energy efficiency, not only for a particular operating point but for the entire battery charging process. Section III involves technologies and battery models to achieve the second optimal performance of minimizing the charging time. The practical thermal limitations of the batteries are included to explain that the conventional constant-current (CC) and constant-voltage (CV) charging mode classification is not appropriate. Within the thermal constraints, the conventional CC mode should practically be replaced by temperature-regulated current-control (TRCC) mode to avoid over-temperature of the battery and achieve minimum charging time. The thermal constraints in the battery imply that an electro-thermal battery model should be used for optimal control for the best charging performance. Section IV describes how the first and second optimal performances can be realized via primary-side control. It explains how real-time battery observers as parts of digital twins can be developed for the primary-side optimal performance control as the fulfillment of the new paradigm shift. Sections V and VI address essential gate-drive and resonator technologies for entering the high-frequency (MHz) and high-power (kW) WPT regime. Finally, the conclusion is provided in Section VII.

II. MAXIMUM EFFICIENCY POINT TRACKING

In the period of the mid-1980s to early-2000s, many WPT research reports pointed to the fact that maximum energy efficiency in a WPT system normally occurs at a particular load condition; however, for battery loads, such load conditions change with the state-of-charge (SoC) of the batteries. As WPT application is extending from a low-power application (e.g., 15 W for fast charging of mobile phones) to high-power applications (e.g., 11 kW for EVs), it is imperative for standard organizations to consider incorporating maximum

energy efficiency tracking (MEET) as a desirable or mandatory feature in their future standards. (Note: MEPT is also known as MEET in some literature. For consistency, it is referred to MEPT in the rest of this article).

It was pointed out in 2014 [5] that the maximum energy efficiency principle, instead of the maximum power transfer theorem [6], should be applied to near-field WPT applications because the latter has the inherent limitation that at least half of the input energy will be wasted in the source resistance. Unlike a photovoltaic system that needs maximum power point tracking, a WPT system requires MEPT [5], [7] because the optimal efficiency operation point changes with the load condition.

A. Basic Principles of MEPT

The MEPT principle is important to WPT for both low-power applications due to the large quantities of portable electronic devices and high-power applications due to high power consumption. In 2014, five research publications reported independent investigations on various ideas of tracking optimal load or tracking maximum efficiency operations [7], [8], [9], [10], [11]. Interestingly, investigation study reports by Zhong and Hui [7], Li et al. [8], and Fu et al. [9] appeared online in August 2014 and as printed versions in the same 2015 issue of the IEEE TRANSACTIONS ON POWER ELECTRONICS. Strictly speaking, the study by Fu et al. [9] is not related to MEPT, because it assumes a source impedance of 50 Ω, and the impedance matching condition is based on the maximum power transfer theorem, as explained in [5]. For this reason, any WPT operation based on the maximum power theorem or impedance matching with a source impedance of 50 Ω cannot achieve energy efficiency higher than 50%. Since [7], [10], and [11] were published, there have been over 50 MEPT-related research publications from 2015 to 2022, according to IEEE Xplore. Some of these publications with different implementation approaches will be highlighted in the following discussion. In general, MEPT can be implemented without [7] and with [8] a wireless communication system.

The basic principle of MEPT is explained here with a simplified equivalent circuit of a series–series (SS) compensated WPT system, as shown in Fig. 3. In the equivalent circuit (Fig. 3) based on fundamental component approximation, v_p is a high-frequency voltage source that is provided by a power inverter. R_{eq} is an equivalent load of the rectifier circuit and battery load. L_p, L_s, and M are the self-inductances and mutual inductance of the coupled coils. C_p and C_s are the compensated capacitors for the primary and secondary circuits, respectively. R_p and R_s are the equivalent series resistances (ESRs) of resonators. The energy transfer efficiency of the WPT system can be calculated by

$$\eta = \frac{\omega^2 M^2 R_{\text{eq}}}{\left[\left(R_s + R_{\text{eq}}\right)^2 + X_s^2\right] R_p + \omega^2 M^2 \left(R_s + R_{\text{eq}}\right)} \tag{1}$$

where $X_s = \omega L_s - (1/\omega C_s)$. According to (1), the energy transfer efficiency of the resonators is determined by four factors: 1) the operating frequency ω, 2) the mutual inductance M, 3) the ESRs of the resonators, i.e., R_p and R_s, and 4) the equivalent load R_{eq}. In general, a higher operating frequency

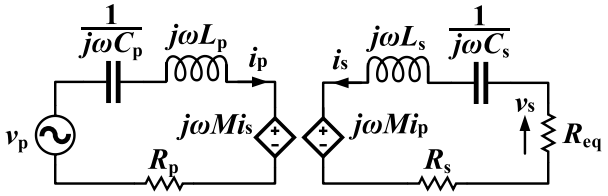

Fig. 3. Equivalent circuit of an SS-compensated WPT system in the frequency domain.

results in a higher energy transfer efficiency that is dependent on the quality (Q) factors of the magnetically coupled coil resonators. The frequency range of WPC-Qi and SAE is in the range of 81.39–300 kHz. The relatively low-equency range was chosen when the power electronics technology was primarily silicon (Si)-based. With the WBG technology and its continuous improvements in the switching speed of power electronics switches, such as gallium nitride (GaN) high electron mobility transistors (HEMTs), it is, however, envisaged that standard organization could increase the operating frequency in the future to reflect the evolution of device technology.

Another way to raise the energy transfer efficiency is to enhance the mutual couplings between the coils via appropriate coil and ferromagnetic designs [12], [13]. The third method to improve energy transfer efficiency is to reduce the ESRs by using coil resonators with high-quality factors. It is, however, worth noting the compromise between the operating frequency and ESRs by considering the skin effects. The fourth solution is to control the equivalent load R_{eq} at the optimal value for MEPT [14], [15], [16]. By equating the derivative of η over R_{eq} to zero, the optimal R_{eq} for MEPT can be derived as

$$R_{\text{eq\_opt}} = R_s \sqrt{1 + \frac{\omega^2 M^2}{R_p R_s}}. \tag{2}$$

Equation (2) forms a fundamental basis for MEPT. Should a mechanism to technically maintain this equivalent optimal load resistance exist over a full range of load variations, any WPT system would achieve MEPT in the entire charging process. A variety of methods can achieve MEPT directly or indirectly based on (2).

Important Remark 1: A more general way to interpret MEPT based on (1) and (2) is to minimize power losses in the ESRs of the transmitter and receiver coil-resonators. The conceptual advancement of the initial MEPT principles in [7], [8], [9], [10], [11] can also be further extended to the total power loss minimization of the entire WPT system, covering the coil-resonators and the power converters on both transmitter and receiver sides, as reflected in subsequent MEPT research publications [17], [18], [19], [20].

B. Methods for Directly or Indirectly Achieving Optimal Load Resistance

Various means have been reported in the literature to provide such a mechanism. Some of these methods are listed as follows.

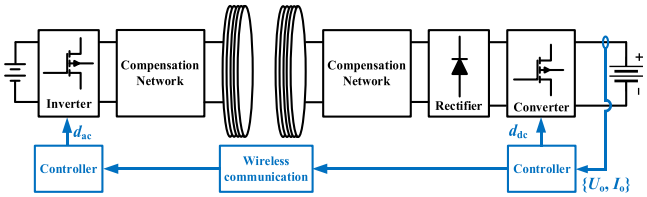

Fig. 4. Schematic of a typical MEPT control strategy with wireless communication from the receiver to the transmitter [8].

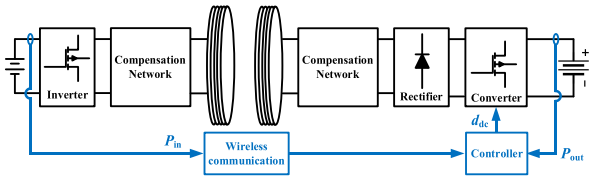

Fig. 5. Schematic of MEPT control for the WPT system with wireless communication from the transmitter to the receiver [9].

Method-1: Use of a dc–dc power converter to emulate the optimal load resistance.

One direct method to emulate the optimal load resistance value is to use duty-cycle control (i.e., $d_{\rm dc}$) of a dc–dc converter that feeds the actual load. Depending on the type of power converter [7], there is a duty-cycle control algorithm that can adjust the input impedance of the dc–dc converter with the load to be equal to the optimal load resistance value, as shown in (2). This duty-cycle control of a dc–dc power converter is a common method used in [7], [8], [9], [15]

$$R_{\rm eq\_opt} = f(d_{\rm dc}, R_L) \tag{3}$$

where R_L is the actual load resistance.

Method-2: Control the primary voltage and secondary voltage of the WPT system.

Ishihara et al. [10] show that the optimal load resistance in (2) can be approximately met by maintaining the voltage ratio of the transmitter and receiver coil-resonators as

$$|v_s|/|v_p| \approx \sqrt{R_s/R_p} \tag{4}$$

where v_p and v_s are the voltages across the transmitter coil and receiver coil, and R_p and R_s are the ESRs of the transmitter coil and receiver coil, respectively. This method is adopted in a slightly different manner in [11] in which the phase angle between v_p and v_s is controlled.

Method-3: Control the primary current and secondary voltage of the WPT system.

It has been pointed out [12] that near-optimal MEPT can be achieved by controlling the phase angle between the transmitter current i_p and the receiver voltage v_s using a phase-locked loop.

C. MEPT Implementations With Wireless Communication System for Feedback Control

In the system shown in Fig. 4, the dc/dc converter on the receiver side is used to regulate the output voltage, and the power inverter on the transmitter side is used to perturb the operating point by changing its conversion ratio $d_{\rm ac}$. The controller records the efficiency for each step and locks into the maximum efficiency point by a perturbation and observation (P&O) method. Another example of MEPT using wireless feedback control is reported in [9] (Fig. 5), even though it uses the power transfer theorem and does not include the power loss in the 50 Ω source impedance. If the WPT system in [9] is modified with a source with near-zero source impedance, the efficiency of the entire WPT system is calculated based on the direct measurements of input and output power. Since the system efficiency (i.e., η) is monotonic with respect to the equivalent resistance (i.e., $R_{\rm eq}$), the optimal duty ratio of the dc–dc converter (which corresponds to the MEPT) can be searched out by the classic P&O method. As the system is dual-monotonic, the P&O control method is robust against parameter drifts and accurate for systems with parasitic parameters since no formula based on the parameters is needed for the controller. It is also designed for the entire WPT system, including the power converters. The control signal is correlated with the control objective directly. The weakness of this method is the need for a wireless communication system. To improve the transient performance, Bosshard et al. [16] proposed a decoupled control method based on the use of proportional–integral (PI) controllers. This scheme requires the wireless feedback of the voltages of the transmitter and receiver coil resonators.

Based on the use of an active rectifier in the receiver circuit, a near-optimal MEPT method is proposed in [21] to operate the WPT system within a range enclosing the maximum efficiency point. Under the CC mode, the transmitter inverter is operated at the resonant frequency of the primary resonator (ω_p), while the active rectifier is operated at a fixed angle of π, like a diode-bridge rectifier. Under the CV mode, the transmitter frequency is increased to a value higher than ω_p to avoid over-voltage, and the angle of the active rectifier will vary under different load conditions. The control scheme in [21] requires a wireless communication link to transfer the equivalent load resistance to the primary side.

There are four variables that can be used to coordinate the transmitter and receiver circuits, namely the frequency and the magnitudes and phase differences of the primary and secondary voltages. Liu et al. [22] proposed a coordinated control of those variables with wireless communication to minimize reactive power in both circuits so as to maximize the energy efficiency. A small amount of reactive power is required in each circuit for zero-voltage switching (ZVS). This approach requires full knowledge of the main circuit and control parameters on both sides, which is suitable for products made by the same manufacturer but unsuitable for the new principle of transferring the optimal control to the transmitter side.

D. MEPT Implementations Without Wireless Communication System for Feedback Control

Fig. 6 shows an original MEPT scheme without using wireless communication [7]. This MEPT principle is simple. For any output power, the duty ratio of the transmitter inverter is adjusted by the P&O method to obtain the minimum input

TABLE II
COMPARISONS AMONG THE ICONIC CONTROL PARADIGMS FOR MEPT OVER THE LAST DECADE

Feature	[10-12]	[9]	[15]	[16]	[7, 22]	[8]	[17, 18]	[19]	[20-22]	[25]	[23, 26]	Future
Efficiency optimization for entire systems	×	×	×	×	√	√	√	√	√	√	√	√
Robustness against parameter drifts and disturbance	×	√	√	√	√	√	√	×	×	×	√	√
No wireless communication	×	×	√	×	√	×	√	√	×	×	√	√
Fast dynamics	√	√	√	√	×	√	×	×	×	√	√	√
Soft switching for all power switches	×	×	×	√	×	√	√	√	√	√	×	√
Compact, reliable and cost-effective receivers	×	×	×	×	×	×	×	×	×	×	×	√

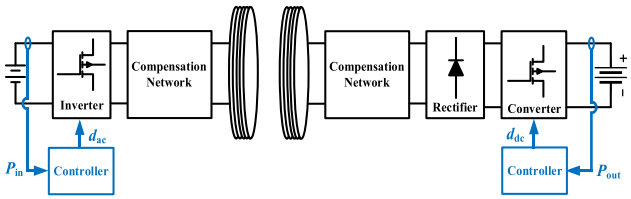

Fig. 6. Schematic of MEPT control for the WPT system without communication [7].

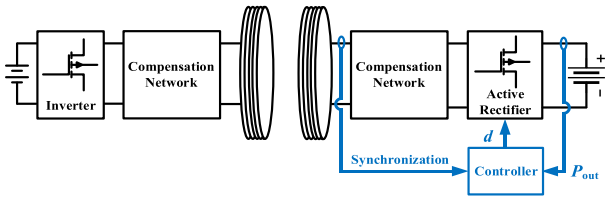

Fig. 7. Schematic of MEPT and ZVS control for the WPT system without communication [19].

power, therefore automatically achieving maximum energy efficiency for the entire WPT system. For any given output power, the input power of the transmitter inverter can be minimized by reaching the minimum input current for a fixed dc inverter voltage or by adjusting the input inverter voltage to its minimum input power if such dc inverter voltage is controllable. Consequently, the MEPT is implemented without any communication between the transmitter and receiver. The transient performance of [7] can be improved with the sliding mode control [23]. Similar control strategies are also adopted for WPT systems with alternative circuits of the dc–dc converter, i.e., active rectifiers [24], [25].

Important Remark 2: The P&O methods used in [7], [8], and [9] are acceptable for static WPT systems (i.e., WPT systems with constant mutual inductances). The typical charging time of a battery load ranges from tens of minutes to several hours, depending on the battery type and capacity. In such a case, the speed of the P&O method is sufficiently fast because the optimal load resistance changes slowly in practice. For dynamic WPT systems where the loads are moving (i.e., WPT systems with dynamically changing mutual inductances), the P&O method for MEPT may not, however, be appropriate. Frequent and fast mutual inductance detection is needed for dynamic WPT unless the wireless charging method is designed to be independent of the mutual inductance [26].

As pointed out in Important Remark 1, the MEPT concept can be extended to consider the power losses in the power converters on both the transmitter and receiver sides. Extending the original MEPT concept to realize ZVS in the transmitter and receiver converters, two approaches have been proposed. One approach is to add auxiliary circuits for the transmitter inverter [27]. This approach can maintain the original control schemes (including the phase shift control). The other approach is to adopt active rectifiers to replace the diode-bridge rectifiers and dc–dc converters, and both MEPT and ZVS can be achieved simultaneously by controlling the phase differences between the control signals of the transmitter and receiver [17], [18], [19], [20]. The schematic of this approach is shown in Fig. 7. By using the active rectifier, the receiver volume and power stages are reduced as compared to the WPT systems with dc–dc regulators. This kind of circuit structure is particularly suitable for bidirectional WPT systems, such as vehicle-to-grid (V2G) WPT systems, while less attractive for the diode-bridge rectifier for one-directional WPT systems. For WPT systems with only diode-bridge rectifiers at the receiver sides, accurate and fast monitoring of mutual inductance or coupling coefficient at the transmitter side without communication feedback from the receiver side is helpful for implementing primary-side control.

The comparison of the MEPT of WPT systems among the iconic control methods of the last decade and the expected control method for the future generation is tabulated in Table II. The future control paradigm can be achieved for the efficiency optimization of WPT systems without any or with minimum wireless communication between the transmitter and receiver if the primary-side control (to be addressed in Section IV) can be widely adopted. Optimal control scheme for the next generation should feature robustness against parameter drifts and disturbance, fast dynamic efficiency tracking, soft switching for all power switches, maximum energy efficiency for the entire charging process, and minimum charging time within the thermal limits of the batteries.

III. MINIMUM CHARGING TIME BASED ON ELECTROTHERMAL LIMITATIONS OF BATTERIES

In the existing literature, optimal wireless charging is often addressed in terms of electrical performance without considering the thermal effects of the batteries. Fig. 8 shows a typical charging profile of a commercial charger for a portable electronic device. The charging profile complies with the Japan Electronics and Information Technology Industries Association (JEITA) guideline [28], which defines the temperature regulations of battery loads. The JEITA standard sets the thermal limits for the charging process of the battery. When the

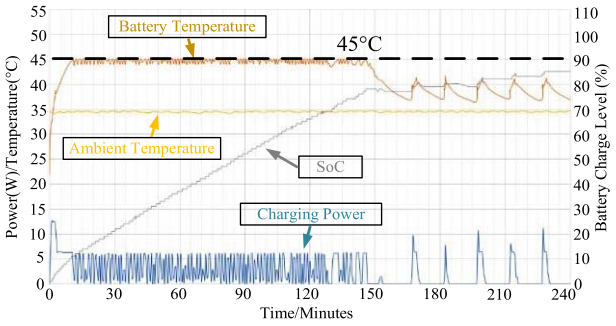

Fig. 8. Practical charging profile of a mobile phone at an ambient temperature of 35 °C (Courtesy of Hong Kong Consumer Council).

TABLE III
SUMMARIES OF PERMISSIBLE TEMPERATURES FOR COMMON RECHARGEABLE BATTERIES [29]

Battery Type	Charge Temp.	Discharge Temp.	Advice
Lead-acid	–20°C to 50°C	–20°C to 50°C	Charge at 0.3C or less below freezing. Lower V-threshold by 3mV/°C when hot.
NiCd and NiMH	0°C to 45°C	–20°C to 65°C	Charge at 0.1C between –18°C and 0°C. Charge at 0.3C between 0°C and 5°C. Charge acceptance at 45°C is 70%. Charge acceptance at 60°C is 45%.
Li-ion	0°C to 45°C	–20°C to 60°C	No charge permitted below freezing. Good charge/discharge performance at higher temperature but shorter life.

first thermal limit is reached, the charging current is reduced by half. When the second thermal limit is reached, the charging current drops to zero to let the battery cool down. The charging power–time profile in Fig. 8 indicates that the charging time is battery-temperature dependent, and the overall charging time, therefore, increases when the battery temperature is near the temperature limits. Fig. 8 shows that it can take over 160 min to charge a mobile phone battery up to an SoC of 80% when the ambient temperature is high. With the charging power battery capacity in the typical range from 40 to 120 kWh for EVs, consideration of the thermal limitations of the batteries is essential in determining the actual charging time of a WPT system.

Table III tabulates the charging and discharge temperature ranges of several common battery types [29]. It is clear that the thermal aspects of the battery must be considered for optimal charging of batteries, not only for minimizing the charging time but also for preserving the lifetime of the batteries.

A. Electrothermal Modeling of Batteries

Recently, research to minimize charging time using a coupled electrothermal battery model and a temperature-regulated

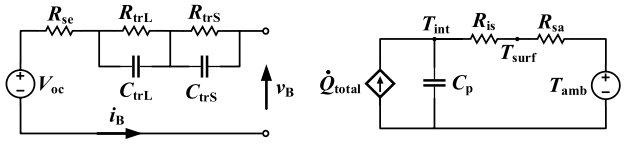

Fig. 9. Coupled electrothermal model of a typical Li-ion battery [30].

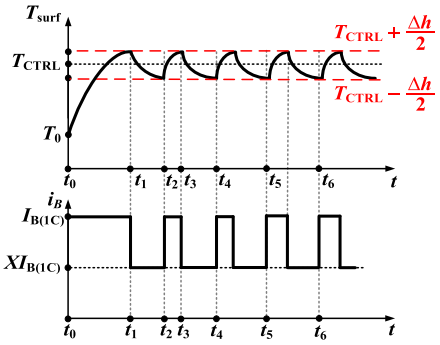

Fig. 10. Typical surface temperature and current profiles of a JEITA-compliant Li-ion battery.

current control was addressed in [30]. The relationships between the charging current and temperature of a typical Li-ion battery can be described by the electrothermal model in Fig. 9. Here, V_{oc} is the open-circuit voltage. v_B and i_B are the instantaneous terminal voltage and charging current, respectively. R_{se} is the internal series resistance. R_{trL} and C_{trL} are the internal slow-dynamic impedance. R_{trS} and C_{trS} are the internal fast-dynamic impedance. In the electrical model, V_{oc}, R_{se}, R_{trL}, C_{trL}, R_{trS}, and C_{trS} are dependent on the SoC of the battery load. In the thermal model, C_p is the heat capacity. R_{is} is the thermal resistance between the internal temperature (i.e., T_{int}) and surface temperature (i.e., T_{surf}) of the battery. R_{sa} is the thermal resistance between T_{surf} and the ambient temperature (i.e., T_{amb}). The total heat generation of the battery (i.e., $\dot{Q}_{total}$) comprises irreversible heat generation (i.e., $\dot{Q}_{irr}$) and reversible heat generation (i.e., $\dot{Q}_{rev}$) [31]. The irreversible heat generation indicates the thermal dissipation on those resistive components (i.e., R_{se}, R_{trL}, and R_{trS}) in the electrical model, which can be calculated by

$$\dot{Q}_{irr} = (v_B - V_{oc})i_B. \tag{5.1}$$

The reversible heat generation is conservative, which can be calculated by

$$\dot{Q}_{rev} = i_B T_{int} \frac{\partial V_{oc}}{\partial T_{int}}. \tag{5.2}$$

Obviously, a Li-ion battery charged by a larger current can result in a higher temperature and vice versa.

B. Temperature-Regulated Current Control Method for Minimizing Charging Time

The schema of typical surface temperature and current profiles of a JEITA-compliant Li-ion battery is depicted in Fig. 10. By considering practical thermal inertia, the hysteresis band ($\Delta h/2$) is adopted for the temperature reference

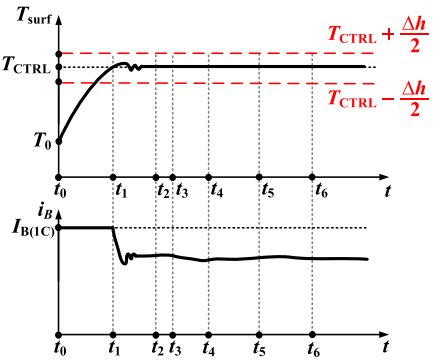

Fig. 11. Typical surface temperature and current profiles of a Li-ion battery with the hybrid temperature-regulated current control.

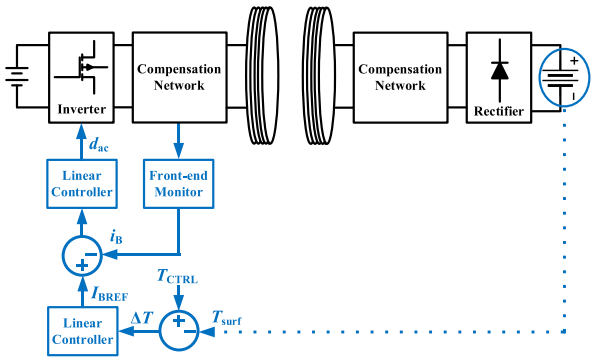

Fig. 12. Primary-side hybrid temperature-regulated current control via amplitude shift keying (ASK) modulation.

T_{CTRL}. When T_{surf} is lower than the lower hysteresis bound [i.e., $T_{surf} < T_{CTRL} - (\Delta h/2)$]), the charging current is controlled at 1C charging current (i.e., $I_{B(1C)}$). Consequently, the surface temperature will rise to the upper hysteresis bound [i.e., $T_{CTRL}+(\Delta h/2)$] during the period from t_0 to t_1. Once the surface temperature reaches the upper bound, the charging current is reduced from $I_{B(1C)}$ to $X \cdot I_{B(1C)}$, where X is a coefficient between 0 and 1 (i.e., $0 < X < 1$). Since the charging current is significantly reduced, the corresponding battery temperature is reduced from the upper bound to the lower bound during the period from t_1 to t_2. When the battery temperature hits the lower bound, the charging current is resumed to 1C. Thereupon, the same procedure repeats until the battery is fully charged. Within the hysteresis band, the charging current remains unchanged. The battery charging speed is determined by the average charging current (i.e., I_{Bavg}). A higher I_{Bavg} can result in a faster charging speed.

The practical charging profile of a mobile phone in Fig. 8 indicates that the conventional CC mode does not hold because the temperature limit cannot be exceeded for safety reasons. To improve the charging speed, a continuous temperature control law is proposed in [30]. The schematic diagrams of typical surface temperature and current profiles of the Li-ion battery with the continuous temperature control law are depicted as shown in Fig. 11. The battery temperature is strictly controlled to track the reference (i.e., T_{CTRL}) by a hybrid temperature-regulated current control, as shown in Fig. 12. With the same root-mean-square (rms) values of the charging currents (the total heat generations are the same), I_{Bavg} of the hybrid temperature-regulated current control is larger than that of the conventional JEITA-compliant control, which means the charging speed can be improved.

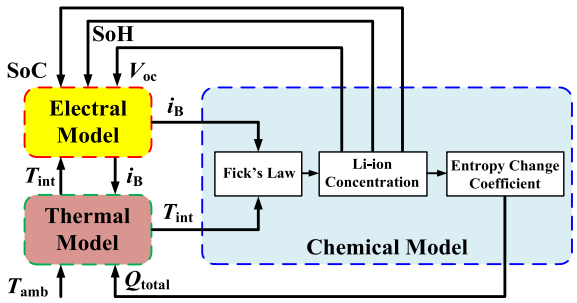

Fig. 13. Electrothermal-chemical model of battery loads for new control methodologies.

In future work, the electrothermal model of the battery load can be upgraded to an electrothermal-chemical model, as shown in Fig. 13. The electrothermal-chemical model, as a part of the battery digital twin, can be established on the transmitter side. The battery voltage and current can be updated based on the primary-side measurements without any fast wireless communication feedback from the receiver side. The hybrid temperature-regulated current control is a practical method that can be adopted on the transmitter side to maximize the charging current of battery loads within the safe thermal limits of the battery. Therefore, it can minimize the charging time in a realistic situation and is an effective solution to meeting one of the optimal performance targets.

IV. Primary-Side Control for Enhancing Interoperability and Optimal Charging Performance

With increasing types of WPT applications, setting new standards to unify a technological platform for enhancing interoperability and simultaneously maintaining optimal performance is desirable. Existing transmitter and receiver controllers of WPT systems are generally designed by different manufacturers. For example, the manufacturer of the wireless charging pad (i.e., transmitter circuit) and the manufacturer of the receiver circuit are often different. While their controller designs are compatible via the design guidelines of international standards, the WPT performance is not optimal. To achieve both optimal performance and compatibility simultaneously, it is necessary for the WPT industry to consider new guidelines for future international standards. The authors are of the view that a paradigm shift of control philosophy is needed to shift most of the control functions of the WPT systems to the primary side, as shown in Fig. 2.

A. First Principle of Primary-Side Control

An early form of primary-side control is reported in [32], which is specific to a WPT system with an inductive-capacitive-inductive (LCL) transmitter circuit and an

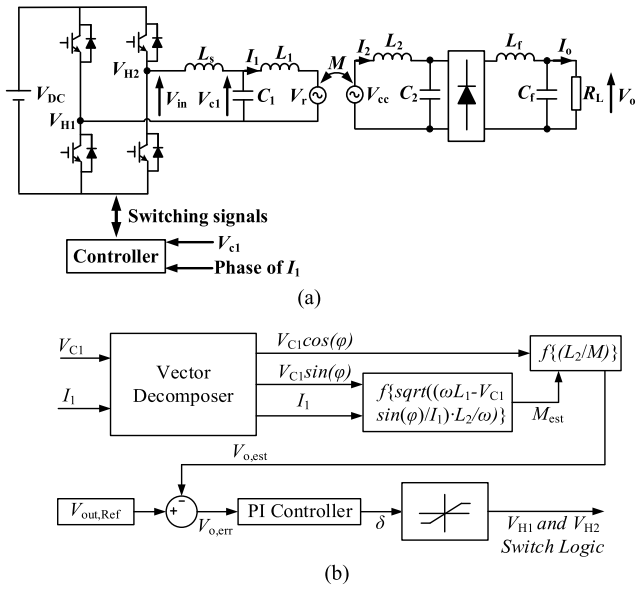

Fig. 14. (a) Primary-side controlled LCL-LC parallel compensated WPT system and (b) its control scheme [32].

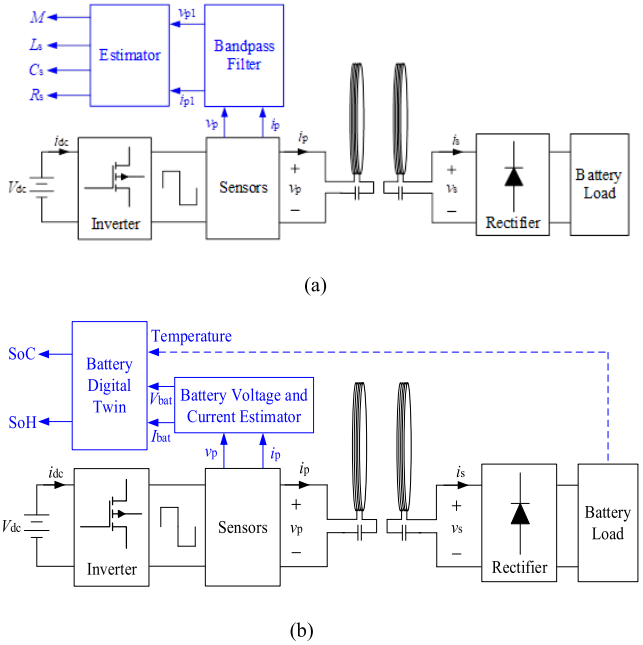

Fig. 15. Schemas of (a) observer and (b) battery digital twin for primary-side control based on the direct measurements in the primary coil-resonator [41].

inductive-capacitive (LC) parallel receiver circuit, as shown in Fig. 14(a). The corresponding control scheme is included in Fig. 14(b). Based on the voltage across the capacitor (C_1) in the LCL circuit and the primary coil current I_1, the capacitor voltage equation can be expressed as real and imaginary parts as follows:

$$V_{c1} = \frac{\pi M}{2\sqrt{2}\ L_2} V_o + j\left(\omega L_1 - \frac{\omega M^2}{L_2}\right) I_1. \tag{6}$$

With I_1 measured on the primary side and L_1 known, the imaginary part of (6) is first used to estimate the mutual inductance M. Then, with the measurement of V_{c1} and the estimated M value, V_o is estimated as the feedback output voltage for comparison with the output voltage reference.

B. General Principle of Primary-Side Control

Without limitation of the topology type, a general approach of primary-side load monitoring and control for a generic WPT system with N-coil resonators was reported in [33] and [34]. The basic idea is to mathematically manipulate the variables in the matrix equations of the WPT systems so that the secondary control variables and parameters (such as the output power, mutual inductance, and load resistance) are expressed in terms of the voltage and current of the transmitter coil resonator [33], [35]. This general approach does not require a wireless communication system to transfer secondary-side variables for feedback control in the primary-side control. It can be extended to multiple-coil-multiple-load WPT systems [36]. Early attempts to estimate the system parameters by using intelligent algorithms are reported in [34] and [37]; however, it takes minutes for intelligent algorithms to determine system parameters. The least-square method provides relatively faster solutions than intelligent algorithms [38]. Fast methods of coupling coefficient detection are addressed in [39] and [40].

This general approach can be expanded so that an observer for the secondary circuit can be constructed on the primary side based on the measurements of the primary current and voltage in the transmitter circuit (Fig. 15) [41]. With the battery digital twin based on the electrothermal-chemical model, a comprehensive primary-side control for the next-generation WPT systems can be depicted, as presented in Fig. 2 [42]. Primary-side control for wireless charging of EVs has been proposed as such an application may financially afford a wireless communication system for WPT feedback control [43]. In the extreme case that the mutual inductance cannot be accurately monitored, primary-side control can still be implemented via the charging-time control (CTC) [26] as a backup.

Important Remark 3: The shift of most of the control functions to the primary side is crucial to the objective of achieving MEPT and minimum charging time in future WPT systems. If adopted in future WPT standards, the manufacturers of the transmitter circuits (e.g., wireless charging pads for mobile phones and EVs) can take the main responsibility for optimizing the charging performance in terms of MEPT and reducing charging time while the manufacturers of the receiver circuits simply focus on the protection aspects of the battery charging process, such as short-circuit and over-temperature protection. The primary-side control, therefore, opens the door to the proposed paradigm shift to enhance system performance while retaining compatibility or interoperability.

V. High-Frequency (Multi-MHz) and High-Efficiency WPT Systems

Contrary to common misconception that magnetic resonance is a recent concept [6], Nicola Tesla used magnetic resonant circuits in his early WPT inventions. It is highlighted in [44] that Tesla emphasized in his early patent documents the use of 1) high operating frequency, 2) low winding resistance,

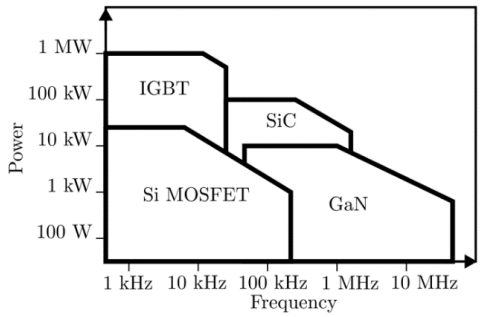

Fig. 16. Power profile of different power electronics switches [45].

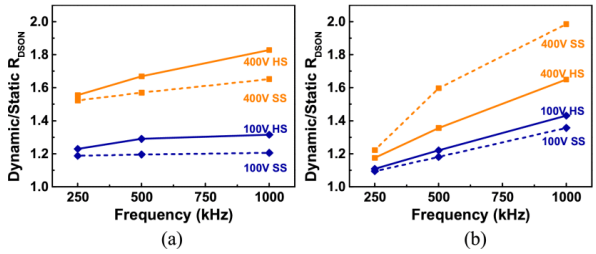

Fig. 17. Dynamic/static R_{DS-on} with different frequencies at 100 and 400 V under hard- and soft-switching conditions. (a) GaN Systems device. (b) Panasonic X-GaN device [49].

and 3) magnetically coupled coils with resonant condensers (i.e., capacitors). In modern terms, Tesla stressed the use of coil-resonators with high quality (Q) factor because the efficiency of a WPT system is proportional to the Q factor. The availability of power MOSFETs in the 1980s offers the required high-frequency voltage sources up to several MHz with the help of a soft-switching technique to realize Tesla's dream of WPT via near-field magnetic resonance. A natural trend for future WPT standards is to increase the operating frequency to achieve high efficiency and high compactness of the WPT systems.

Based on the Si and its super junction (SJ) semiconductor technology, the frequency of the SAE J2954 standard is set at 85 ($\pm$5%) kHz for EV charging applications while that of Qi at a frequency up to about 300 kHz. The recent advances of WBG power devices [45], such as silicon carbide (SiC) and GaN HEMT switch devices (Fig. 16), open the doors to extend the WPT applications to high power and high operating frequency beyond the 10 MHz regimes, respectively. With continuous advancements of power electronics, the operating frequencies would increase in stages in future standards. To break into the uncharted territory of the high-frequency (multi-MHz) and high-power region (Fig. 1) for future WPT applications, several key issues must be tackled [46], [47].

A. Power Losses Versus Operating Frequency for Power Switches

At multi-MHz operation, the 1) *conduction loss*, 2) *overlap switching loss*, 3) *displacement loss*, and 4) *gating loss* of the power switches should be considered. While GaN HEMT is superior to Si-based power switches in terms of the advantages of zero reverse recovery, lower switching energy, and faster switching speed [46], the current collapse issue (also known as the dynamic R_{DS-on} issue) caused by high voltage stress and off-state duration can drastically increase the R_{DS-on} by $\sim$1.5 times to more than two times and the problem deteriorates at higher frequencies [48], [49], [50]. Depending on the device technology, some types of GaN devices have lower dynamic R_{DS-on} at hard-switching compared to soft-switching under higher voltage stresses (such as the Panasonic X-GaN), while some do not show many differences (such as GaN System's GS 650V family [49]) (Fig. 17).

The *overlap switching loss* can be mitigated by applying soft-switching techniques, particularly for multi-MHz operation [46]. GaN HEMT devices have much smaller C_{OSS}, C_{ISS}, and Q_G values than Si devices and thus have shorter switch transitions and lower switching loss at the turn-off transition. The total capacitance across the switching device in the circuit is normally large enough to reduce the rate of change of V_{DS} and it acts like a natural turn-off snubber. Therefore, only ZVS turn-on is needed for the GaN switches [51], [52]. For WPT systems driven by half-bridge or full-bridge inverters, the equivalent impedance seen by the inverter circuit shall be tuned to slightly inductive so that the lagging load current drives the voltage across opposing switch(es) to zero before they are turned on [53].

The *displacement loss* is mainly taken place due to voltage swings across the blocking substrate when the device is kept off. For the currently available and popular devices, such as GaN-HEMT, there is unexpected extra losses associated with the C_{OSS}, which contributes to additional power losses on the device [54], [55]. This loss cannot be mitigated with any external circuit operations but is intrinsic to the device materials. In [54], the improved device structure (additional III-N buffer layers) is suggested. But it is uncertain if device manufacturers would adopt such techniques at the expense of other aspects of device performance and costs. Perera et al. [55] indicate that the loss tangent (δ) is constant to the device family and can be used as a figure of merit for selecting switching devices. Such a loss also applies to capacitors connected in shunt to the switches, such as the multilayer ceramic capacitors (MLCCs) used for adjusting ZVS quasi-resonant times.

Last, the *gating loss* is generally improved in WBG devices as the drive voltage and gate charge are reduced. It is given by

$$P_G = Q_G V_{GS} f. \tag{7}$$

For instance, a couple of representative devices are listed and evaluated with their gating loss at 10 MHz in Table IV.

To mitigate gating losses where SiC or Si devices are selected, gate energy recycling techniques [56], [57] may be used at an additional cost of complexity in control and fine-tuning of the inductor, as illustrated in Fig. 18. A combination of GaN HEMT and SiC devices can mitigate the drawbacks of both types. In [58], a cascode WBG heterogeneous power device is proposed and verified in an experiment

TABLE IV

GATING LOSS AT RECOMMENDED V_{GS} AND 10 MHZ FOR COMMONLY USED GAN HEMT COMPARED TO SIC AND SI(SJ) DEVICES

Device	Type	$V_{(BL)DSS}$ (V)	R_{DS-on} (mΩ)	Q_G (nC)	V_{GS} (V)	P_G (W)
GS66504B	GaN	650	100	3.3	6	0.198
EPC2204	GaN	100	6	5.7	5	0.285
PGA26E07BA	GaN	600	56	5.0	12	0.6
C3M0045065K	SiC	650	45	63	15	9.45
IPI65R190C	Si(SJ)	650	190	68	10	6.8

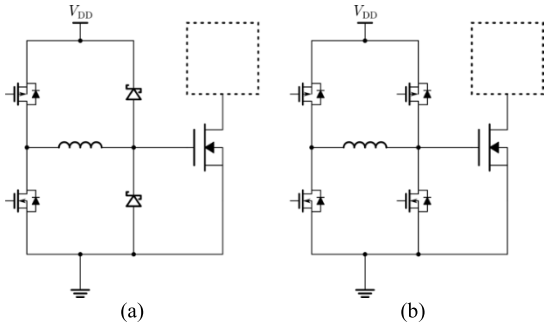

Fig. 18. Resonant gate driver with energy recovery. (a) Chen et al. [56] and (b) Eberle et al. [57].

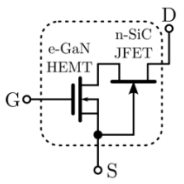

Fig. 19. Cascode GaN/SiC device consists of a GaN HEMT and a SiC JFET [58].

using commercial-grade components, as shown in Fig. 19. The hybrid device in a 700 W class-E inverter operates at 13.56 MHz with a gating loss of 558 mW and an overall efficiency of 91%. It retains the advantages of high voltage blockage and low C_{OSS} losses of SiC devices, and low gating loss and simple gate driver design of GaN devices at the same time.

B. Signal Integrity

At high frequencies, the signal integrity can be compromised, causing additional power losses and possibly operational or device failures. Besides additional losses, several worth-noting phenomena may have substantial impacts on the power conversion circuits in WPT systems.

The fast rising/falling edges contain a very wide spectrum of frequency components, which are inevitably distorted or delayed by parasitics, and the nonlinearity of the stray capacitances requires additional care. For example, it is common to use large input resistors, such as 100 kΩ, in the op-amps used for downscaling voltage and current waveforms in WPT systems. A stray capacitance of 3 pF to ground after the resistor makes it a low-pass filter with a cut-off frequency at 530 kHz and a phase shift of 71.5° at 1.5 MHz [59].

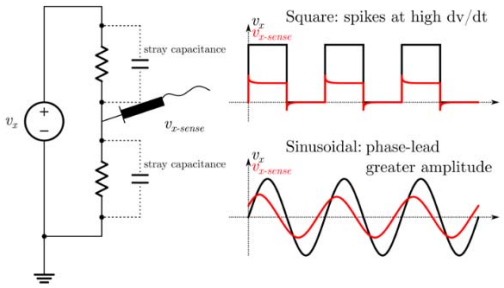

Fig. 20. Distortions on voltage divider at high frequencies due to stray capacitances.

A second example is that a simple voltage divider circuit cannot properly function at high slew rates as expected due to the stray capacitance across the resistors, as shown in Fig. 20. Proper compensation at the operating frequency by adding larger capacitances to dilute the stray capacitances can mitigate the issue.

A third example is the false turn-on when V_{DS} rises too fast, and the displacement current charges the gate up and accidentally turns the gate on, which causes additional losses [60], [61]. This problem is further severed by nonlinearities in the capacitances, which cannot be accurately estimated and compensated by external components. In many cases, manual trimming with low-granularity components is necessary.

Another worth-noting issue comes with the common-mode transient immunity (CMTI) capability of the isolators used in the half-bridge or full-bridge inverters [62]. A large dv/dt transient at the floating side can trigger a false turn-on signal for the switch and cause shoot-throughs. It is recommended to use the latest gate drives with dedicated optimizations on the common-mode noise rejection rates (CMNR) [63], [64].

C. Electromagnetic Interference (EMI)/Electromagnetic Compatibility (EMC) Considerations

Both conducted and radiated EMI issues need to be considered. For conducted EMI, it is relatively easy to filter the high-frequency components to meet the regulations. Regulations, such as CISPR 22, EN55022, and IEC/EN61000-3-2, have specified allowable noise levels from 150 kHz [65]. For the radiated emissions, the regulations differ among geographical regions. In the United States, uses of frequencies above 9 kHz are subject to Federal Communications Commission (FCC) rules and need approval under Part 15, Part 18, or both. Wireless charging systems that operate below 100 kHz must not exceed 83 V/m of electric field and 90 A/m of a magnetic field in external areas, while those above 100 and 300 kHz are subject to a specific absorption rate (SAR) (1.6 W/kg) and maximum permissible exposure (MPE) limits, respectively [66]. The spatial field strengths can be evaluated and visualized by multiphysics tools, such as ANSYS and COMSOL, during the design stage [67]. Normally high-intensity areas occur near the windings, which should be shielded by a casing. Among the multi-MHz frequency range, many works selected the industrial, scientific, and medical (ISM) bands of 6.78,

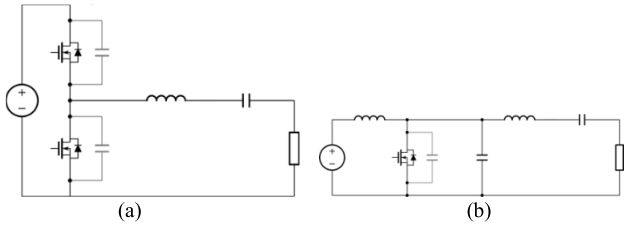

Fig. 21. Two major classes of circuit topologies used for WPT systems. (a) Class-D/DE configuration. (b) Class-E configuration.

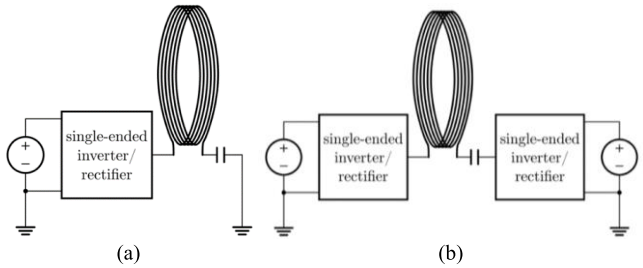

Fig. 22. (a) Single- and (b) double-ended connections for windings.

13.56, 27.12, and 40.68 MHz; however, the use of these bands is still subject to local regulations and authorizations, and existing communication devices may not tolerate the intensive interference as the ISM bands were initially set for wireless communication purposes only.

D. Topological Considerations and the State-of-the-Art

Two major classes of topologies are often seen in the inverter and rectifier designs for WPT systems, namely the class-D/DE and the class-E/ϕ2 power amplifiers, as depicted in Fig. 21. Conventional class-D inverters are simply hard-switched half-bridges [68], and the early implementations achieve zero current switchings (ZCS) to mitigate the switching losses. The class-DE inverters use the lagging current in the inductive load to achieve zero voltage and zero dv/dt switching [69], so that the ON-transition switching loss is mitigated to the minimum. A similar operation can be applied to the rectifier converters used at the receiving end. Both class-D and -DE circuits utilize the full voltage-blocking capability of the switching devices. Note that the class-D/DE family requires high/low side gate drives, and both switches in a leg need to have matched latencies in the level-shift/gate drive paths. This may affect the maximum operating frequency in some feedback-type ZVS systems as the latency is in series in the loop. A variant of the class-D/DE type is the current mode class-D (CMCD) inverters [70]. It has the advantages of all switches referenced to the ground and better load and parameter tolerance due to the half-sine voltage waveforms ensuring ZVS at both turn-on and off. The self-coupled winding design is, however, technically challenging, as reported in [71].

The class-E [72] and the later improved version, the class-ϕ2 (also known as the class-EF_2 in some literatures) [73], [74] are single-switch soft-switching implementations with additional series resonant circuits that are free from the floating gate driver problems. The switches in such circuits, however, experience excessive stress (2×–3.6×) from the resonance operation that wastes available $V_{(BL)DSS}$ on the device. For the existing GaN HEMT devices, this high-voltage stress worsens the losses associated with the dynamic R_{DS-on} and C_{OSS} loss issues.

For various types of circuit topologies, the load (winding) can be connected in either a single-ended or double-ended way, as shown in Fig. 22. The single-ended connection benefits from the low cost and the simplicity of the circuits. The double-ended connection doubles the equivalent driving voltage to the load when the source voltage is fixed. At a high frequency, a mismatch in the circuit parameters on the two sides may cause an imbalance of voltage stresses on components.

TABLE V
STATE-OF-THE-ART MULTI-MHZ WPT SYSTEMS

Ref	Topology	Frequency	Device	VDC	Power	Efficiency
[71]	CMCD	27.12MHz	GaN	21 V	101.9W	89.6%
[76]	CMCD	100MHz	GaN	15 V	6.9W	81.9%
[77]	Class-φ2	13.56MHz	GaN	280 V	1.3kW	95%
[78]	Class-φ2	27.12MHz	Si	40 V	25W	75%
[79]	Class-φ2	13.56MHz	GaN	240 V	618W	84%
[80]	Class-φ2	6.78MHz	GaN	-	1.7kW	95.7%

A selection of recent representative multi-MHz inductive WPT systems over a wide range of voltage, power, and frequency is included for comparison in Table V. Some recent works on class-D type inverters also have great potential for WPT systems. A 1 kW 13.56 MHz ZVS class-D inverter with variable-load operation can achieve a peak of 95.4% efficiency in [51]. Based on the same operating principle, a multiinverter discrete-backoff (MIDB) configuration of multiple inverters using a coaxial cable transformer power combiner is proposed for 5 kW, 13.56 MHz operations using 650V GaN devices [52], [75]. With the recent advancement of fast gate drive circuits with short latency (<10 ns) for soft-switched half-bridge and full-bridge power inverters [106], operating WPT systems at tens of megahertz is feasible even for kilowatts applications

VI. VERSATILE AND HIGH-EFFICIENT RESONATOR DESIGNS

The next-generation WPT is also looking at a design paradigm shift for the resonator designs. Previously the product design needed to be adapted to accommodate the resonator circuits provided by WPT designers or to use commercially available off-the-shelf (COTS) ones, such as those in Table I; however, this often results in an ineffective use of either the products' enclosure spaces, such as fitting a circular winding into a rectangle box case; or/and an inadequate power capability of the circuits, such as using a pair of resonators rated higher power ratings than the actual power demand. Versatile resonators customized to the applications will be needed, and the following points are to be addressed.

1) Adaptations of winding designs to fit the products' enclosures.

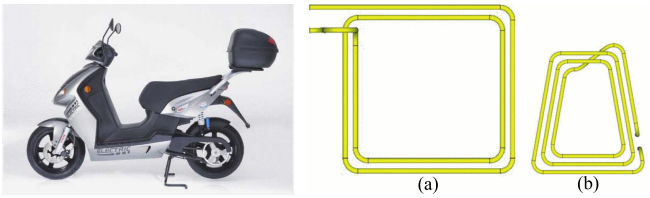

Fig. 23. Windings used in the wireless charger for E-scooters [79], [84] (Copyright @ IEEE). (a) Transmitter coil. (b) Receiver coil.

2) Optimizations for minimum angular/linear misalignment disturbances, either through the change of shapes or by applying multiple resonator configurations.

3) Optimizations for minimum power losses in the resonator circuits.

A. Windings Fitting the Irregular Enclosures

Windings can be arranged in irregular shapes so that the aperture sizes and the mutual coupling are maximized. Examples are the trapezoidal multiturn receiver winding in [79] (Fig. 23) and wireless power provisioning over spherical structures [81], [82], [83].

The evaluation of self- and mutual-inductance values for irregular windings then plays a key role in design and optimizations. 3-D finite-element method (FEM) software, such as ANSYS and COMSOL, are normally used; however, the manual 3-D modeling and evaluations often take minutes to hours for a design candidate. To speed up the process, the trajectory of the winding can be generated by programming. Numerical solvers based on Neumman's formula (8), such as [85] and artificial intelligence (AI)-based optimization, such as [86], offer fast and accurate results compared to 3-D FEM software. In [87], a parametric search and spatial sampling evaluation can help determine the optimal shape of a cone-shaped Tx winding for an even distribution of power delivery over an observation area. The whole process takes several minutes on a normal laptop computer. This brings better efficiency and convenience in parametric optimizations for irregular windings

$$L_{S,M} = \frac{\mu_0}{4\pi} \oint \oint \frac{dx \cdot dx'}{|dx - dx'|}. \tag{8}$$

B. Multiresonator for Misalignment Tolerance

Multiple numbers of winding and their subsidiary circuits can be jointly used at both the transmitter and receiver sides to tackle a range of free angular and/or linear displacement [88]. The basic principles can be elaborated in a vector combination way based on the paradigm of the three-orthogonal circular winding structure [89]. A closed-form theoretical maximum efficiency for multiple transmitter single receiver systems is derived based on the Cauchy–Schwartz inequality in [90] and similar conclusions in MagMIMO [91] (Fig. 24) using the maximal-ratio combining method. In practice, these structures are often restricted by the form factors of the product, e.g., a flat structure like a mobile phone. Some alternative variations can solve the angular and lateral misalignment

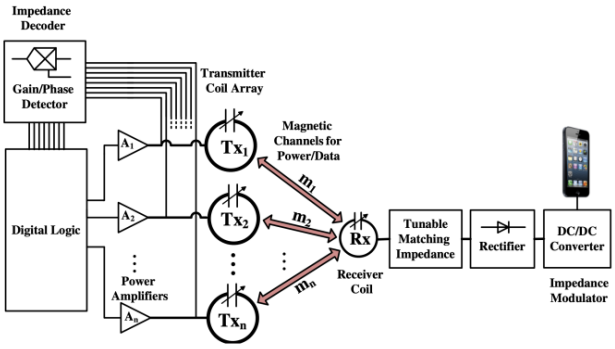

Fig. 24. Block diagram of MagMIMO prototype [91].

issues [92], [93], [94]. For example, the two crossed dipole structure is a good solution to achieve 6-degree-of-freedom WPT with completely planar designs on both Tx and Rx sides, meeting the minimum requirements of uninterrupted power supply at free moves [93].

C. Considerations for Megahertz Resonator Construction

An objective in resonator design is the maximization of the Q factor. The losses associated with the winding structure are due to the *skin effect*, the *proximity effect*, the *fringing effect* (where crossings of wires take place), and the *hysteresis/eddy loss* in the core/shielding materials if there are any. Litz wires are often used to mitigate the losses due to the skin effect. The proximity effect also, however, takes place within the stranded bundle [95]. Therefore, in many high-power multi-MHz WPT systems, copper tube coils are often used [47], [79], as the expansion of radius still effectively increases the conduction area. A multiturn winding has unevenly distributed current densities over the cross-sectional area due to the proximity effect when multiple turns are packed [96]. On the other hand, closely packing the turns result in more parasitic capacitances [97] that lowers the self-resonant frequency of the winding, and the current through the leakage capacitance reduces the induced magnetic field [98]. The printed circuit board (PCB) coils [99], including the flexible printed circuit (FPC) types [100], are often used in low-power applications for consistency in manufacturing tolerance and inexpensive production cost. Special care is needed to reduce the stray capacitance in a multilayer spiral coil to increase the useable bandwidth for inductor/transformer windings [101]; however, this characteristic can be utilized to form a natural resonator where discrete capacitors cannot be installed due to high electric fields [102]. The operational characteristic of such a winding design is discussed in [103], where both proximity effect and interlayer displacement current (leakage) take place at the same time, as shown in Fig. 25.

Printing two planar windings on two sides of a PCB board means that the dielectric property of the PCB material will form the equivalent capacitance, which limits the resonant frequency. A recent advancement of using new PCB structures as resonators for megahertz WPT applications is reported in [104] to further reduce the intercapacitance and intracapacitance of the spiral PCB windings so that the resonant

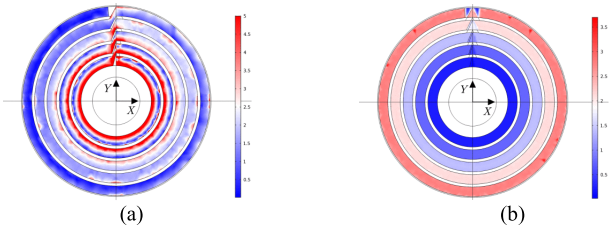

(a) (b)

Fig. 25. (a) Surface conduction current density and (b) interlayer displacement current density in a two-layer PCB winding [103].

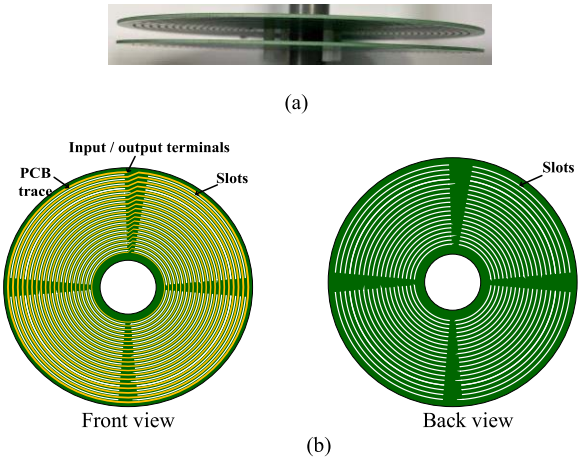

(a)

(b)

Fig. 26. Structure of a new PCB resonator with reduced intercapacitance and intracapacitance for megahertz WPT applications [104]. (a) Side view of a new PCB resonator formed by two PCBs with an air gap. (b) Front and back view of each PCB board.

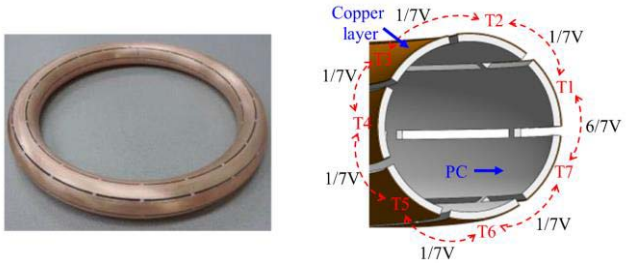

(a) (b)

Fig. 27. Resonator based on a 3-D printed surface spiral winding (with seven turns) for megahertz and kilowatts WPT applications [105]. (a) Photograph and (b) voltage distribution (Copyrights @ IEEE).

frequency can reach the megahertz range. This new structure comprises two planar PCB windings arranged in a sandwiched structure with a middle layer of airgap [Fig. 26(a)]. The electric field passes through the airgap instead of the PCB material, therefore resulting in a reduction of interwinding capacitance. In addition, air trenches (slots) are made between adjacent turns of the PCB windings in both planar windings to reduce the intrawinding capacitance [Fig. 26(b)]. In the study reported in [104], the quality factor, resonant frequency, and transmission efficiency of the new designs are significantly improved by over 410%, 240%, and 88%, respectively, over those of the conventional designs. Future resonator designs for high-frequency operation may benefit from electroplating and 3-D printing technologies. A good example (Fig. 27) is the surface spiral winding printed on the surface of a circular tube of polycarbonate (PC) for high-frequency (MHz) and high-power (kW) applications [105]. Given different application scenarios, the suggested strategies are summarized in Table VI.

TABLE VI
SUMMARY OF RESONATOR DESIGN STRATEGIES

Scenario	Strategy	Example
Irregular enclosure shape	Warp the winding into irregular shapes to maximize the aperture size.	[79][84], tools:[85]
Stable power delivery over misalignment	Tweaking the shape of the windings	[87]
	Using multiple Tx and/or Rx windings	[91]-[95]
Multi-megahertz operations, high-Q resonators	Using hollow copper tubes to make windings	[47][79]
Need low-cost windings; good consistency of inductance values; constraints of thin form factor	Using PCB windings; sometimes can use intrinsic stray capacitance as natural compensation.	[99] - [103]

VII. CONCLUSION

With the increasing power level and range of WPT applications, there is a need for a paradigm shift to optimal performance to achieve high system efficiency and minimum charging time for the entire charging process of the battery loads without compromising interoperability. This article highlights some essential concepts and technologies that can be incorporated for such a paradigm shift in future WPT standards. By transferring most of the control functions to the transmitter side based on the digital twins at the primary side, the manufacturers of the transmitter circuit (i.e., chargers) can be responsible for the optimal control, while the manufacturers of the receiver circuits only need to deal with key protective functions, such as short-circuit and over-temperature protection of the battery loads, while the fast communication feedbacks are not required. The state-of-the-art technologies and the challenges in breaking into the multi-MHz and high-power WPT regimes are addressed. New gate drives with short latency for soft-switched power inverters will be essential to high-frequency and high-power WPT applications. The WBG power devices and new technologies for printed resonators would offer practical solutions to enter this unchartered territory.

REFERENCES

[1] Statista. *Size of Wireless Charging Market Worldwide From 2020 to 2030*. Accessed: Jun. 23, 2022. [Online]. Available: https://www.statista.com/statistics/1256342/worldwide-wireless-charging-market-revenues

[2] *Wireless Power Consortium Website*. Accessed: Jun. 23, 2022. [Online]. Available: https://www.wirelesspowerconsortium.com

[3] *Wireless Power Transfer for Light-Duty Plug-in/Electric Vehicles and Alignment Methodology*, SAE Standard J2954, Oct. 2020.
[4] AirFuel Alliance. *Wireless Charging Technology & Standardshttps*. Accessed: Jun. 23, 2022. [Online]. Available: http://airfuel.org
[5] S. Y. R. Hui, W. Zhong, and C. K. Lee, "A critical review of recent progress in mid-range wireless power transfer," *IEEE Trans. Power Electron.*, vol. 29, no. 9, pp. 4500–4511, Sep. 2014.
[6] A. Kurs, A. Karalis, R. Moffatt, J. D. Joannopoulos, P. Fisher, and M. Soljačić, "Wireless power transfer via strongly coupled magnetic resonances," *Science*, vol. 317, no. 5834, pp. 83–86, 2007.
[7] W. X. Zhong and S. Y. R. Hui, "Maximum energy efficiency tracking for wireless power transfer systems," *IEEE Trans. Power Electron.*, vol. 30, no. 7, pp. 4025–4034, Jul. 2015.
[8] H. Li, J. Li, K. Wang, W. Chen, and X. Yang, "A maximum efficiency point tracking control scheme for wireless power transfer systems using magnetic resonant coupling," *IEEE Trans. Power Electron.*, vol. 30, no. 7, pp. 3998–4008, Jul. 2015.
[9] M. Fu, H. Yin, X. Zhu, and C. Ma, "Analysis and tracking of optimal load in wireless power transfer systems," *IEEE Trans. Power Electron.*, vol. 30, no. 7, pp. 3952–3963, Jul. 2015.
[10] H. Ishihara et al., "A voltage ratio-based efficiency control method for 3 kW wireless power transmission," in *Proc. IEEE Appl. Power Electron. Conf. Expo.*, Fort Worth, TX, USA, Mar. 2014, pp. 1312–1316.
[11] F. Pellitteri, V. Boscaino, R. Miceli, and U. K. Madawala, "Power tracking with maximum efficiency for wireless charging of E-bikes," in *Proc. IEEE Int. Electr. Vehicle Conf. (IEVC)*, Florence, Italy, Dec. 2014, pp. 1–7.
[12] M. Budhia, G. A. Covic, and J. T. Boys, "Design and optimization of circular magnetic structures for lumped inductive power transfer systems," *IEEE Trans. Power Electron.*, vol. 26, no. 11, pp. 3096–3108, Nov. 2011.
[13] W. Zhang, J. C. White, A. M. Abraham, and C. C. Mi, "Loosely coupled transformer structure and interoperability study for EV wireless charging systems," *IEEE Trans. Power Electron.*, vol. 30, no. 11, pp. 6356–6367, Nov. 2015.
[14] W. Zhang, S.-C. Wong, C. K. Tse, and Q. Chen, "Load-independent duality of current and voltage outputs of a series- or parallel-compensated inductive power transfer converter with optimized efficiency," *IEEE J. Emerg. Sel. Topics Power Electron.*, vol. 3, no. 1, pp. 137–146, Mar. 2015.
[15] M. Fu, C. Ma, and X. Zhu, "A cascaded boost–buck converter for high efficiency wireless power transfer systems," *IEEE Trans. Ind. Informat.*, vol. 10, no. 3, pp. 1972–1980, Aug. 2014.
[16] R. Bosshard, J. W. Kolar, and B. Wunsch, "Control method for inductive power transfer with high partial-load efficiency and resonance tracking," in *Proc. Int. Power Electron. Conf.*, May 2014, pp. 2167–2174.
[17] H. Li, J. Fang, S. Chen, K. Wang, and Y. Tang, "Pulse density modulation for maximum efficiency point tracking of wireless power transfer systems," *IEEE Trans. Power Electron.*, vol. 33, no. 6, pp. 5492–5501, Jun. 2018.
[18] H. Li, K. Wang, J. Fang, and Y. Tang, "Pulse density modulated ZVS full-bridge converters for wireless power transfer systems," *IEEE Trans. Power Electron.*, vol. 34, no. 1, pp. 369–377, Jan. 2019.
[19] F. Xu, S.-C. Wong, and C. K. Tse, "Inductive power transfer system with maximum efficiency tracking control and real-time mutual inductance estimation," *IEEE Trans. Power Electron.*, vol. 37, no. 5, pp. 6156–6167, May 2022.
[20] Y. Jiang, L. Wang, J. Fang, C. Zhao, K. Wang, and Y. Wang, "A joint control with variable ZVS angles for dynamic efficiency optimization in wireless power transfer system," *IEEE Trans. Power Electron.*, vol. 35, no. 10, pp. 11064–11081, Oct. 2020.
[21] Z. Huang, S.-C. Wong, and C. K. Tse, "An inductive-power-transfer converter with high efficiency throughout battery-charging process," *IEEE Trans. Power Electron.*, vol. 34, no. 10, pp. 10245–10255, Oct. 2019.
[22] Y. Liu, U. K. Madawala, R. Mai, and Z. He, "An optimal multivariable control strategy for inductive power transfer systems to improve efficiency," *IEEE Trans. Power Electron.*, vol. 35, no. 9, pp. 8998–9010, Sep. 2020.
[23] Y. Yang, W. Zhong, S. Kiratipongvoot, S.-C. Tan, and S. Y. R. Hui, "Dynamic improvement of series–series compensated wireless power transfer systems using discrete sliding mode control," *IEEE Trans. Power Electron.*, vol. 33, no. 7, pp. 6351–6360, Jul. 2018.
[24] X. Tang, J. Zeng, K. P. Pun, S. Mai, C. Zhang, and Z. Wang, "Low-cost maximum efficiency tracking method for wireless power transfer systems," *IEEE Trans. Power Electron.*, vol. 33, no. 6, pp. 5317–5329, Jun. 2018.
[25] R. Mai, Y. Liu, Y. Li, P. Yue, G. Cao, and Z. He, "An active-rectifier-based maximum efficiency tracking method using an additional measurement coil for wireless power transfer," *IEEE Trans. Power Electron.*, vol. 33, no. 1, pp. 716–728, Jan. 2018.
[26] W. Zhong and S. Y. R. Hui, "Charging time control of wireless power transfer systems without using mutual coupling information and wireless communication system," *IEEE Trans. Ind. Electron.*, vol. 64, no. 1, pp. 228–235, Jan. 2017.
[27] Y. Yang and S. Y. R. Hui, "An augmented passive circuit for soft-switching of power inverter under phase-shift modulation control," Tech. Rep., 2021.
[28] Japan Electronics and Information Technology Industries Association and Battery Association of Japan. (2007). *A Guide to the Safe Use of Secondary Lithium Ion Batteries in Notebook-Type Personal Computers*. [Online]. Available: https://home.jeita.or.jp/page_file/20110517171451_cub9MvYFEh.pdf
[29] Battery University. *BU-410: Charging at High and Low Temperature*. Accessed: Jun. 23, 2022. [Online]. Available: https://batteryuniversity.com/article/bu-410-charging-at-high-and-low-temper
[30] H.-W.-R. Liang, Y. Yang, and S. Y. R. Hui, "Improvement of lithium-ion battery charging from the state-of-the-art industrial JEITA guidelines to a hybrid temperature-regulated current control," *IEEE Trans. Power Electron.*, vol. 37, no. 6, pp. 6412–6423, Jun. 2022.
[31] M. Balasundaram, V. Ramar, C. Yap, L. Li, A. A. O. Tay, and P. Balaya, "Heat loss distribution: Impedance and thermal loss analyses in $LiFePO_4$/graphite 18650 electrochemical cell," *J. Power Sources*, vol. 328, pp. 413–421, Oct. 2016.
[32] D. J. Thrimawithana and U. K. Madawala, "A primary side controller for inductive power transfer systems," in *Proc. IEEE Int. Conf. Ind. Technol.*, Via del Mar, Chile, Mar. 2010, pp. 661–666.
[33] J. Yin, D. Lin, C. K. Lee, and S. Y. R. Hui, "Load monitoring and output power control of a wireless power transfer system without any wireless communication feedback," in *Proc. IEEE Energy Convers. Congr. Expo.*, Denver, CO, USA, Sep. 2013, pp. 4934–4939.
[34] D. Lin, J. Yin, and S. Y. R. Hui, "Parameter identification of wireless power transfer systems using input voltage and current," in *Proc. IEEE Energy Convers. Congr. Expo. (ECCE)*, Pittsburgh, PA, USA, Sep. 2014, pp. 832–836.
[35] J. Yin, D. Lin, C.-K. Lee, and S. Y. R. Hui, "A systematic approach for load monitoring and power control in wireless power transfer systems without any direct output measurement," *IEEE Trans. Power Electron.*, vol. 30, no. 3, pp. 1657–1667, Mar. 2015.
[36] J. Yin, D. Lin, C. Kwan Lee, T. Parisini, and S. Y. Hui, "Front-end monitoring of multiple loads in wireless power transfer systems without wireless communication systems," *IEEE Trans. Power Electron.*, vol. 31, no. 3, pp. 2510–2517, Mar. 2016.
[37] J. P.-W. Chow, H.-H. Chung, C.-S. Cheng, and W. Wang, "Use of transmitter-side electrical information to estimate system parameters of wireless inductive links," *IEEE Trans. Power Electron.*, vol. 32, no. 9, pp. 7169–7186, Sep. 2017.
[38] J. Yin, D. Lin, T. Parisini, and S. Y. R. Hui, "Front-end monitoring of the mutual inductance and load resistance in a series–series compensated wireless power transfer system," *IEEE Trans. Power Electron.*, vol. 31, no. 10, pp. 7339–7352, Oct. 2016.
[39] Y. Yang, S. C. Tan, and S. Y. R. Hui, "Fast hardware approach to determining mutual coupling of series–series-compensated wireless power transfer systems with active rectifiers," *IEEE Trans. Power Electron.*, vol. 35, no. 10, pp. 11026–11038, Oct. 2020.
[40] J. Zeng, S. Chen, Y. Yang, and S. Y. R. Hui, "A primary-side method for ultrafast determination of mutual coupling coefficient in milliseconds for wireless power transfer systems," *IEEE Trans. Power Electron.*, vol. 37, no. 12, pp. 15706–15716, Dec. 2022.
[41] S. Y. R. Hui and D. Lin, "Methods for parameter identification, load monitoring and output power control in wireless power transfer systems," U.S. Patent 20 224 751 B2, Mar. 5, 2019.
[42] S. Y. R. Hui and Y. Yang, "A method for controlling battery charging mode," Patent PCT/CN2020/090 939, May 19, 2020.
[43] J. M. Miller, O. C. Onar, and M. Chinthavali, "Primary-side power flow control of wireless power transfer for electric vehicle charging," *IEEE J. Emerg. Sel. Topics Power Electron.*, vol. 3, no. 1, pp. 147–162, Mar. 2015.

[44] S. Y. R. Hui, "Magnetic resonance for wireless power transfer [a look back]," *IEEE Power Electron. Mag.*, vol. 3, no. 1, pp. 14–31, Mar. 2016.

[45] M. Beheshti, "Wide-bandgap semiconductors: Performance and benefits of GaN versus SiC," *Analog Des. J.*, vol. 4, pp. 1–6, Jan. 2020. [Online]. Available: https://www.ti.com/lit/an/slyt801/slyt801.pdf

[46] D. J. Perreault et al., "Opportunities and challenges in very high frequency power conversion," in *Proc. IEEE Appl. Power Electron. Conf. Expo. (APEC)*, Washington, DC, USA, Feb. 2009, pp. 1–14.

[47] M. Pinuela, D. C. Yates, S. Lucyszyn, and P. D. Mitcheson, "Maximizing DC-to-load efficiency for inductive power transfer," *IEEE Trans. Power Electron.*, vol. 28, no. 5, pp. 2437–2447, May 2013.

[48] C. Roy and B. Parkhideh, "Design consideration for characterization and study of dynamic on state resistance of GaN devices," in *Proc. IEEE 7th Workshop Wide Bandgap Power Devices Appl. (WiPDA)*, Raleigh, NC, USA, Oct. 2019, pp. 181–186.

[49] R. Li, X. Wu, S. Yang, and K. Sheng, "Dynamic on-state resistance test and evaluation of GaN power devices under hard- and soft-switching conditions by double and multiple pulses," *IEEE Trans. Power Electron.*, vol. 34, no. 2, pp. 1044–1053, Feb. 2019.

[50] K. Li, P. Evans, and M. Johnson, "GaN-HEMT dynamic ON-state resistance characterisation and modelling," in *Proc. IEEE 17th Workshop Control Modeling Power Electron. (COMPEL)*, Trondheim, Norway, Jun. 2016, pp. 1–7.

[51] W. D. Braun and D. J. Perreault, "A high-frequency inverter for variable-load operation," *IEEE J. Emerg. Sel. Topics Power Electron.*, vol. 7, no. 2, pp. 706–721, Jun. 2019.

[52] H. Zhang, A. A. Bastami, A. S. Jurkov, A. Radomski, and D. J. Perreault, "Multi-inverter discrete backoff: A high-efficiency, wide-range RF power generation architecture," in *Proc. IEEE 21st Workshop Control Modeling Power Electron. (COMPEL)*, Aalborg, Denmark, Nov. 2020, pp. 1–8.

[53] J. A. Sabate, V. Vlatkovic, R. B. Ridley, F. C. Lee, and B. H. Cho, "Design considerations for high-voltage high-power full-bridge zero-voltage-switched PWM converter," in *Proc. 5th Annu. Appl. Power Electron. Conf. Expo.*, Los Angeles, CA, USA, 1990, pp. 275–284.

[54] M. Guacci, "On the origin of the C_{oss}-losses in soft-switching GaN-on-Si power HEMTs," *IEEE J. Emerg. Sel. Top. Power Electron.*, vol. 7, no. 2, pp. 679–694, Oct. 2019.

[55] N. Perera et al., "C_{oss} loss tangent of field-effect transistors: Generalizing high-frequency soft-switching losses," *IEEE Trans. Power Electron.*, vol. 35, no. 12, pp. 12585–12589, Dec. 2020.

[56] Y. Chen, F. C. Lee, L. Amoroso, and H. Wu, "A resonant MOSFET gate driver with efficient energy recovery," *IEEE Trans. Power Electron.*, vol. 19, no. 2, pp. 470–477, Mar. 2004.

[57] W. Eberle, Y.-F. Liu, and P. C. Sen, "A new resonant gate-drive circuit with efficient energy recovery and low conduction loss," *IEEE Trans. Ind. Electron.*, vol. 55, no. 5, pp. 2213–2221, May 2008.

[58] J. Xu, L. Gu, Z. Ye, S. Kargarrazi, and J. M. Rivas-Davila, "Cascode GaN/SiC: A wide-bandgap heterogenous power device for high-frequency applications," *IEEE Trans. Power Electron.*, vol. 35, no. 6, pp. 6340–6349, Jun. 2020.

[59] R. S. Burwen, "How to design analog circuits without a computer or a lot of paper," in *Analog Circuit Design: Art, Science and Personalities*, J. Williams, Ed., Boston, MA, USA: Elsevier, 1991, pp. 149–167.

[60] M. R. Ahmed, R. Todd, and A. J. Forsyth, "Predicting SiC MOSFET behavior under hard-switching, soft-switching, and false turn-on conditions," *IEEE Trans. Ind. Electron.*, vol. 64, no. 11, pp. 9001–9011, Nov. 2017.

[61] R. Xie, H. Wang, G. Tang, X. Yang, and K. J. Chen, "An analytical model for false turn-on evaluation of high-voltage enhancement-mode GaN transistor in bridge-leg configuration," *IEEE Trans. Power Electron.*, vol. 32, no. 8, pp. 6416–6433, Aug. 2017.

[62] W. Zhang and M. Begue. (2018). *Common Mode Transient Immunity (CMTI) for UCC2122x Isolated Gate Drivers*. Texas Instruments. [Online]. Available: https://www.ti.com/lit/an/slua909/slua909.pdf

[63] X. Ke and D. B. Ma, "A 3-to-40 V V_{IN} 10-to-50 MHz 12 W isolated GaN driver with self-excited t_{dead} minimizer achieving 0.2 ns/0.3 ns t_{dead}, 7.9% minimum duty ratio and 50 V/ns CMTI," in *IEEE Int. Solid-State Circuits Conf. (ISSCC) Dig. Tech. Papers*, San Francisco, CA, USA, Feb. 2018, pp. 386–387.

[64] R. Yun, J. Sun, E. Gaalaas, and B. Chen, "A transformer-based digital isolator with 20 kVPK surge capability and >200 kV/μS common mode transient immunity," in *Proc. IEEE Symp. VLSI Circuits (VLSI-Circuits)*, Honolulu, HI, USA, Jun. 2016, pp. 1–2.

[65] D. Li and J. Schnabel. (2019). *Electromagnetic Compatibility Considerations for Switched-Mode Power Supplies*. CUI Inc. Accessed: Jul. 4, 2022. [Online]. Available: https://www.cui.com/catalog/resource/download/emi-considerations-for-switching-power-supplies.pdf

[66] Laboratory Division, Office of Engineering and Technology, Federal Communications Commission. (Jan. 27, 2021). *RF Exposure Considerations for Low Power Consumer Wireless Power Transfer Applications*. Accessed: Jul. 4, 2022. [Online]. Available: https://apps.fcc.gov/kdb/GetAttachment.html?id=g5f2nQFxHnlMbja%2FFzq1QQ%3D%3D&desc=680106%20D01%20RF%20Exposure%20Wireless%20Charging%20Apps%20v03r01&tracking_number=41701

[67] C. Zhang, W. Zhong, X. Liu, and S. Y. R. Hui, "A fast method for generating time-varying magnetic field patterns of mid-range wireless power transfer systems," *IEEE Trans. Power Electron.*, vol. 30, no. 3, pp. 1513–1520, Mar. 2015.

[68] P. J. Baxandall, "Transistor sine-wave LC oscillators," *Proc. IEE*, vol. 106, no. 16, pp. 748–758, 1959.

[69] D. C. Hamill, "Class DE inverters and rectifiers for DC–DC conversion," in *Proc. 27th Annu. IEEE Power Electron. Spec. Conf.*, Baveno, Italy, Jul. 1996, pp. 854–860.

[70] H. Kobayashi, J. M. Hinrichs, and P. M. Asbeck, "Current-mode class-D power amplifiers for high-efficiency RF applications," *IEEE Trans. Microw. Theory Techn.*, vol. 49, no. 12, pp. 2480–2485, Dec. 2001.

[71] J. Rademacher, X. Zan, and A. Avestruz, "High power, high efficiency wireless power transfer at 27.12 MHz using CMCD converters," in *Proc. IEEE Energy Convers. Congr. Expo. (ECCE)*, Vancouver, BC, Canada, Oct. 2021, pp. 5698–5703.

[72] N. O. Sokal and A. D. Sokal, "Class E–A new class of high-efficiency tuned single-ended switching power amplifiers," *IEEE J. Solid-State Circuits*, vol. SSC-10, no. 3, pp. 168–176, Jun. 1975.

[73] J. M. Rivas, Y. Han, O. Leitermann, A. D. Sagneri, and D. J. Perreault, "A high-frequency resonant inverter topology with low-voltage stress," *IEEE Trans. Power Electron.*, vol. 23, no. 4, pp. 1759–1771, Jul. 2008.

[74] J. M. Rivas, O. Leitermann, Y. Han, and D. J. Perreault, "A very high frequency DC–DC converter based on a class-2 resonant inverter," *IEEE Trans. Power Electron.*, vol. 26, no. 10, pp. 2980–2992, Oct. 2011.

[75] H. Zhang et al., "Modeling and design of high-power non-isolating RF power combiners based on transmission lines," in *Proc. IEEE Appl. Power Electron. Conf. Expo. (APEC)*, Houston, TX, USA, Mar. 2022, pp. 259–266.

[76] X. Zan and A.-T. Avestruz, "100 MHz symmetric current-mode class D wireless power transfer," *IEEE J. Emerg. Sel. Topics Power Electron.*, vol. 35, no. 12, pp. 12678–12685, Dec. 2020.

[77] J. Choi, D. Tsukiyama, Y. Tsuruda, and J. M. R. Davila, "High-frequency, high-power resonant inverter with eGaN FET for wireless power transfer," *IEEE Trans. Power Electron.*, vol. 33, no. 3, pp. 1890–1896, Mar. 2018.

[78] S. Aldhaher, D. C. Yates, and P. D. Mitcheson, "Design and development of a class EF_2 inverter and rectifier for multimegahertz wireless power transfer systems," *IEEE Trans. Power Electron.*, vol. 31, no. 12, pp. 8138–8150, Dec. 2016.

[79] C. H. Kwan, J. M. Arteaga, S. Aldhaher, D. C. Yates, and P. D. Mitcheson, "A 600 W 6.78 MHz wireless charger for an electric scooter," in *Proc. IEEE PELS Workshop Emerg. Technol., Wireless Power Transf. (WoW)*, Seoul, South Korea, Nov. 2020, pp. 278–282.

[80] L. Gu and J. Rivas-Davila, "1.7 kW 6.78 MHz wireless power transfer with air-core coils at 95.7% DC–DC efficiency," in *Proc. IEEE Wireless Power Transf. Conf. (WPTC)*, San Diego, CA, USA, Jun. 2021, pp. 1–4.

[81] W. Zhou and S. Huang, "An accurate model for fast calculating the resonant frequency of an irregular solenoid," *IEEE Trans. Microw. Theory Techn.*, vol. 67, no. 7, pp. 2663–2673, Jul. 2019.

[82] C. Zhang, D. Lin, and S. Y. R. Hui, "Ball-joint wireless power transfer systems," *IEEE Trans. Power Electron.*, vol. 33, no. 1, pp. 65–72, Jan. 2018.

[83] M. A. Houran, X. Yang, and W. Chen, "Two-degree-of-freedom WPT system using cylindrical-joint structure for applications with movable parts," *IEEE Trans. Circuits Syst. II, Exp. Briefs*, vol. 68, no. 1, pp. 366–370, Jan. 2021.

[84] (2019). *Govecs GO! S2.4—Electric Moped Scooter*. [Online]. Available: https://www.e-scooter.co/govecs-go-s2-4/

[85] C. Zhang, X. Chen, K. Chen, and D. Lin, "IPTVisual: Visualisation of the spatial energy flows in inductive power transfer systems with arbitrary winding shapes," *World Electr. Vehicle J.*, vol. 13, no. 4, p. 63, Apr. 2022.

[86] W. O. Adepoju, I. Bhattacharya, M. E. Bima, and T. Banik, "Novel metamaterial and AI-based multi-objective optimization of coil parameters for efficient wireless power transfer," in *Proc. IEEE Vehicle Power Propuls. Conf. (VPPC)*, Oct. 2021, pp. 1–6.
[87] C. Zhang, "A design methodology for irregularly shaped windings in inductive wireless power transfer systems," *Electronics*, vol. 11, no. 22, p. 3754, Nov. 2022, doi: 10.3390/electronics11223754.
[88] W. M. Ng, C. Zhang, D. Lin, and S. Y. Ron Hui, "Two- and three-dimensional omnidirectional wireless power transfer," *IEEE Trans. Power Electron.*, vol. 29, no. 9, pp. 4470–4474, Sep. 2014.
[89] C. Zhang, D. Lin, and S. Y. Hui, "Basic control principles of omnidirectional wireless power transfer," *IEEE Trans. Power Electron.*, vol. 31, no. 7, pp. 5215–5227, Jul. 2016.
[90] C. Zhang, D. Lin, and S. Y. R. Hu, "Efficiency optimization method of inductive coupling wireless power transfer system with multiple transmitters and single receiver," in *Proc. IEEE Energy Convers. Congr. Expo. (ECCE)*, Sep. 2016, pp. 1–6, doi: 10.1109/ECCE.2016.7855071.
[91] J. Jadidian and D. Katabi, "Magnetic MIMO: How to charge your phone in your pocket," in *Proc. 20th Annu. Int. Conf. Mobile Comput. Netw.*, Sep. 2014, pp. 495–506, doi: 10.1145/2639108.2639130.
[92] E. S. Lee, J. S. Choi, H. S. Son, S. H. Han, and C. T. Rim, "Six degrees of freedom wide-range ubiquitous IPT for IoT by DQ magnetic field," *IEEE Trans. Power Electron.*, vol. 32, no. 11, pp. 8258–8276, Nov. 2017.
[93] B. H. Choi, E. S. Lee, Y. H. Sohn, G. C. Jang, and C. T. Rim, "Six degrees of freedom mobile inductive power transfer by crossed dipole Tx and Rx coils," *IEEE Trans. Power Electron.*, vol. 31, no. 4, pp. 3252–3272, Apr. 2016.
[94] Z. Zhang and B. Zhang, "Angular-misalignment insensitive omnidirectional wireless power transfer," *IEEE Trans. Ind. Electron.*, vol. 67, no. 4, pp. 2755–2764, Apr. 2020.
[95] Z. Liu, J. Zhu, and L. Zhu, "Accurate calculation of eddy current loss in Litz-wired high-frequency transformer windings," *IEEE Trans. Magn.*, vol. 54, no. 11, pp. 1–5, Nov. 2018.
[96] A. W. Lotfi and F. C. Lee, "A high frequency model for Litz wire for switch-mode magnetics," in *Proc. Conf. Rec. IEEE Ind. Appl. Conf. Twenty-Eighth IAS Annu. Meeting*, Toronto, ON, Canada, Oct. 1993, pp. 1169–1175.
[97] A. Massarini, "Analytical approach to the calculation of parasitic capacitance between winding turns," in *Proc. IEEE 4th Int. Forum Res. Technol. Soc. Ind. (RTSI)*, Palermo, Italy, Sep. 2018, pp. 1–4.
[98] Z. Shafiq, J. Xia, Q. Min, S. Li, and S. Lu, "Study of the induced electric field effect on inductive power transfer system," in *Proc. IEEE PELS Workshop Emerg. Technol., Wireless Power Transf. (WoW)*, San Diego, CA, USA, Jun. 2021, pp. 1–5.
[99] S. C. Tang, S. Y. R. Hui, and H. S.-H. Chung, "Coreless planar printed-circuit-board (PCB) transformers—A fundamental concept for signal and energy transfer," *IEEE Trans. Power Electron.*, vol. 15, no. 5, pp. 931–941, Sep. 2000.
[100] G. K. Y. Ho, C. Zhang, B. M. H. Pong, and S. Y. R. Hui, "Modeling and analysis of the bendable transformer," *IEEE Trans. Power Electron.*, vol. 31, no. 9, pp. 6450–6460, Sep. 2016.
[101] C. K. Lee, Y. Su, and S. Y. R. Hui, "Printed spiral winding inductor with wide frequency bandwidth," *IEEE Trans. Power Electron.*, vol. 26, no. 10, pp. 2936–2945, Oct. 2011.
[102] J. Qu, S. Kiratipongvoot, C. K. Lee, and N. Tang, "An integrated printed-circuit-board resonator design for inductive power transfer system," in *Proc. IEEE Energy Convers. Congr. Expo. (ECCE)*, Portland, OR, USA, Sep. 2018, pp. 2021–2025.
[103] Y. Fang, J. Qu, B. M. H. Pong, C. K. Lee, and R. S. Y. Hui, "Quasi-static modeling and optimization of two-layer PCB resonators in wireless power transfer systems for 110-kV power grid online monitoring equipment," *IEEE Trans. Ind. Electron.*, vol. 69, no. 2, pp. 1400–1410, Feb. 2022.
[104] K. A. Li and S. Y. R. Hui, "Printed-circuit-board inductive-capacitive resonators for high frequency operation," Patent 10 202 300 104 Y, Jan. 13, 2023.
[105] G. Zhu and R. D. Lorenz, "Surface spiral parallel and antiparallel winding designs for high efficiency, low spatial voltage stress, and inductive wireless power transfer systems," *IEEE Trans. Ind. Appl.*, vol. 55, no. 1, pp. 741–750, Jan. 2019.
[106] C. Zhang and S. Y. R. Hui, "Gate drive system and power control method for soft switching of power inverter with operating frequency up to tens of mega-Hertz," Patent 10 202 250 496 N, Jul. 18, 2022.

Shu-Yuen Ron Hui (Fellow, IEEE) received the B.Sc. (Eng) degree (Hons.) in electrical and electronic engineering from the University of Birmingham, Birmingham, U.K., in 1984 and the D.I.C. and Ph.D. degrees in electrical engineering from the Imperial College London, London, U.K., in 1987.

He was previously a Philip Wong Wilson Wong Professor with the University of Hong Kong, Hong Kong. He currently holds the MediaTek Endowed Professorship with Nanyang Technological University, Singapore, and a Chair Professorship of power electronics with the Imperial College London. He has published over 500 research articles, including 320 refereed journal publications. Over 120 of his patents have been adopted by industry worldwide. His research interests include power electronics, wireless power, sustainable lighting, and smart grid. His inventions on wireless charging platform technology underpin key dimensions of Qi, the world's first wireless power standard, with freedom of positioning and localized charging features for wireless charging of consumer electronics. He also developed the Photo-Electrothermal Theory for light-emitting-diode (LED) Systems.

Dr. Hui is a Fellow of the Australian Academy of Technological Sciences and Engineering, U.S. National Academy of Inventors, and Royal Academy of Engineering, U.K. He received the IEEE Rudolf Chope Research and Development Award and the IET Achievement Medal (The Crompton Medal) in 2010, and IEEE William E. Newell Power Electronics Award in 2015.

Yun Yang (Member, IEEE) received the B.Sc. degree in electrical engineering from Wuhan University, Wuhan, China, in 2012 and the Ph.D. degree in electrical engineering from the University of Hong Kong, Hong Kong, in 2017.

He was a Research Assistant Professor with the Department of Electrical Engineering, The Hong Kong Polytechnic University, Hong Kong. He is currently an Assistant Professor with the School of Electrical and Electronic Engineering, Nanyang Technological University, Singapore. His research interests include wireless power transfer, renewable energy technologies, electric vehicles, power electronics, and advanced control.

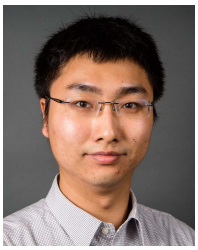

Cheng Zhang (Member, IEEE) was born in China, in 1990. He received the B.Eng. degree (Hons.) in electronic and communication engineering from the City University of Hong Kong, Hong Kong, in 2012 and the Ph.D. degree in electronic and electrical engineering from The University of Hong Kong, Hong Kong, in 2016.

From 2016 to 2017, he was a Senior Research Assistant with the Department of Electrical and Electronic Engineering, The University of Hong Kong. He was a Post-Doctoral Research Associate with the Research Laboratory of Electronics, Massachusetts Institute of Technology, Cambridge, MA, USA, from 2017 to 2018. He is currently working as a Lecturer in power electronics with the University of Manchester, Manchester, U.K. His research interests include high-frequency ac–dc power conversions and designs and optimizations for wireless power transfer applications.